Asian Journal of Chemistry; Vol. 25, No. 16 (2013), 9203-9207

ASIAN JOURNAL OF CHEMISTRY

http://dx.doi.org/10.14233/ajchem.2013.15148

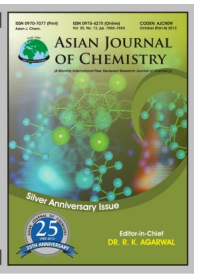

Investigation on High-Temperature Decomposition and Regeneration Characteristics of Hydroxyapatite Powders and Sinters

RENFU QUAN[1,*], CHUNYAN WANG[2], HONGBIN WANG[2], XICHENG WEI[2] and ZHIJUN ZHAO[2]

[1]Department of Orthopaedics, Xiaoshan Traditional Chinese Medical Hospital, Hangzhou 311201, P.R. China
[2]School of Materials Science and Engineering, Shanghai University, Shanghai 200072, P.R. China

*Corresponding author: E-mail: quanrenfu8@163.com; rfquan@163.com

(*Received*: 15 January 2013; *Accepted*: 20 September 2013) AJC-14145

Hydroxyapapite has been widely used because of its excellent biocompatibility. In this work, we studied the decomposition characteristics of both nano-hydroxyapapite powders prepared by the precipitation method and the corresponding sinters at the temperature from room temperature to 1500 ºC. X-Ray diffractometer, Raman spectroscopy and high temperature differential scanning calorimeter were employed to investigate the decomposition characteristics. Results show that hydroxyapapite powders gradually release the OH^- ions from 1000 ºC and decompose into β-tricalcium phosphate (β-TCP) and tetracalcium phosphate (TTCP) when the heating temperature is higher than 1360 ºC and the β-TCP phase changes into α-TCP at about 1450 ºC, which remains if the sinter cools to the room temperature. We also found that the decomposed sinters can reconstitute to hydroxyapapite again under a slow cooling rate and in a certain atmosphere. This work revealed and compared the decomposition and regeneration characteristics of hydroxyapapite powders and sinters, which is useful for the applications of hydroxyapapite materials.

Key Words: Hydroxyapatite, Calcium phosphate, Decomposition, Regeneration.

INTRODUCTION

Hydroxyapatite [$Ca_{10}(PO_4)_6(OH)_2$], the main mineral constituent of human bone, is widely investigated for clinical applications because of the excellent biocompatibility, fast bone regeneration ability and direct bonding to regenerated bone without intermediate connective tissue[1-4]. Various bioceramics materials based on hydroxyapapite such as ordered macroporous hydroxyapapite have been reported[5], which may find applications in fields such as bone regeneration because of their interconnected porosity like other ordered porous materials[6]. However, it is generally accepted that the thermal stability and mechanical properties of hydroxyapapite cannot fully satisfy the requirements of clinical applications[7,8]. To this end, surface coatings by spraying or forming composite materials have been applied to hydroxyapapite[9]. For example, Wen and Kung[10] developed high quality hydroxyapapite coated polyether ether ketone composites by gas plasma spray. Two different types of hydroxyapapite powders were used in the plasma spray system and they found that the smaller and spherical hydroxyapapite powder produced hydroxyapapite coating with lower surface roughness. A suitable buffer layer such as Ti deposition has been quite effective in improving the hydroxyapatite coating quality, which was ascribed to the improved wettability and heat conductivity. It should be noted that the processing temperature in these treatments is usually higher than the decomposition temperature of hydroxyapapite, leading to the decomposition or transformation of hydroxyapatite. For example, hydroxyapapite can transform to tricalcium phosphate [$Ca_3(PO_4)_2$, TCP] or oxyhydroxyapatite [$Ca_{10}(PO_4)_6(OH)_2$] at elevated temperature[11]. Previously we employed pressure-less sintering method to prepare ZrO_2/hydroxyapapite composite ceramics at 1600 ºC and found that the decomposition phase on the surface was TCP and tetracalcium phosphate ($Ca_4P_2O_9$, TTCP)[12]. The decomposition of hydroxyapapite at high temperature have hampered its large scale applications as coatings or composite materials.

It is important to investigate the decomposition behaviours of hydroxyapapite. Liao *et al.*[11] studied the thermal decomposition and reconstitution of hydroxyapatite powder and confirmed the decomposition temperature of hydroxyapapite powder. Lin *et al.*[13] also observed the reconstitution behavior of quenched hydroxyapatite powder and they found that the quenched hydroxyapatite powder could be partly transformed to hydroxyapatite in the air again[13]. Few researchers have studied the decomposition of hydroxyapatite block and sinters and compared with hydroxyapatite powder, which are important for the actual applications. In this work, we investigated and compared the high-temperature decomposition and regeneration characteristics of both hydroxyapatite powders and sinters.

EXPERIMENTAL

$Ca(NO_3)_2{\cdot}4H_2O$ and $(NH_4)_3PO_4{\cdot}3H_2O$, as raw materials of analytical grade, were used to prepare nano-hydroxyapatite powders by the method of precipitation[14]. The resultant nano-hydroxyapatite powers was drying for about 3 h at 110 ºC in a DHG-9070 drying cabinet before use. High resolution transmission electron microscope (JEM-2010F, TEM) was employed to observe the morphology of the hydroxyapatite powers.

The hydroxyapatite block with a diameter of 18.9 mm was formed by pressing on a CMT-530 type universal tester under a pressure of 100 MPa at room temperature. The loading rate was 200 N/s. The specimen was kept for 180 s under the maximum pressure and then was put into YFA12/16G-Y chamber electric resistance furnace and sintered at different temperatures in the air.

To study the regeneration behaviour, a hydroxyapatite block was erected in a home-made closed box containing $NaHCO_3$ (0.5 g and 1 g). The regeneration reaction box was heated at 900 ºC for 1 h followed by cooling to room temperature. During the regeneration, the box was sealed with refractory clay and asbestos, so that the decomposition products (CO_2 and water vapor) of $NaHCO_3$ were able to contact fully with the hydroxyapatite block.

D\max-2550 X-ray diffractometer (XRD) with CuK_α radiation was employed to detect the crystalline structure of hydroxyapatite power and its sinters. The range of scanning angle was from 20-40º with a speed of 4º/min. Raman spectra was recorded at 400, 700, 750, 800, 900, 1000, 1100, 1200, 1300 and 1350 ºC using HR LabRAM800 high temperature Raman spectroscopy to evaluate the functional group of hydroxyapatite. NETZSCH DSC 404C high temperature differential scanning calorimeter (DSC) was used to study the thermal behaviour of hydroxyapatite. The scanning temperature was from room temperature to up to 1550 ºC with a heating rate of 10 ºC/min and the gas flow rate is 50 mL/min.

RESULTS AND DISCUSSION

Hydroxyapatite (HA) powders were prepared from $Ca(NO_3)_2{\cdot}4H_2O$ and $(NH_4)_3PO_4{\cdot}3H_2O$ by the method of precipitation. Fig. 1 shows TEM micrograph and XRD pattern of the resultant hydroxyapatite powders. It can be seen from Fig. 1(a) that the hydroxyapatite powders are less than 100 nm in length and are rod-shaped. Fig. 1(b) demonstrates the crystal phase transformation for the nano-hydroxyapatite powders. The diameter of the hydroxyapatite block is 18.9 mm and it shrank to 13.4 mm after sintered. The shrinkage rate was *ca.* 29 %.

Fig. 2 is the high-temperature DSC curve of hydroxyapatite powder. A series of peaks can be seen from the curve. It is known that there are two kinds of water in hydroxyapatite that was prepared by the method of precipitation, *i.e.*, the absorbed and the crystallization water. The absorbed water was lost at the temperature of 50-200 ºC. When the temperature increases to 200-400 ºC, the loss of crystallization water occurred. The exothermic peaks at 720 and 901 ºC are caused by the crystallization process. The huge endothermic peak indicates the loss of OH^- ion and the decomposition of

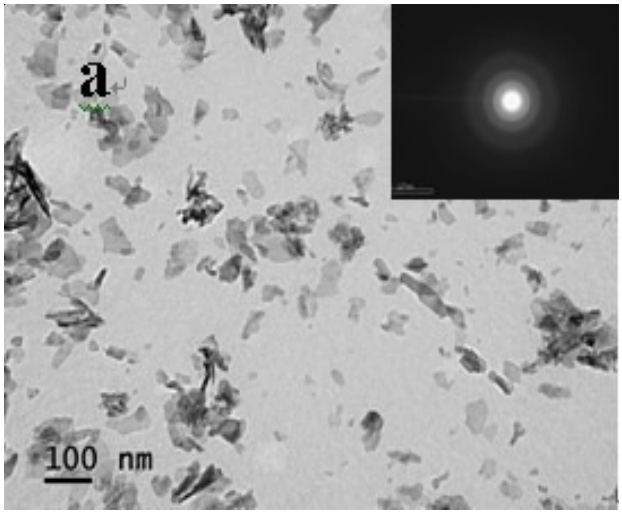

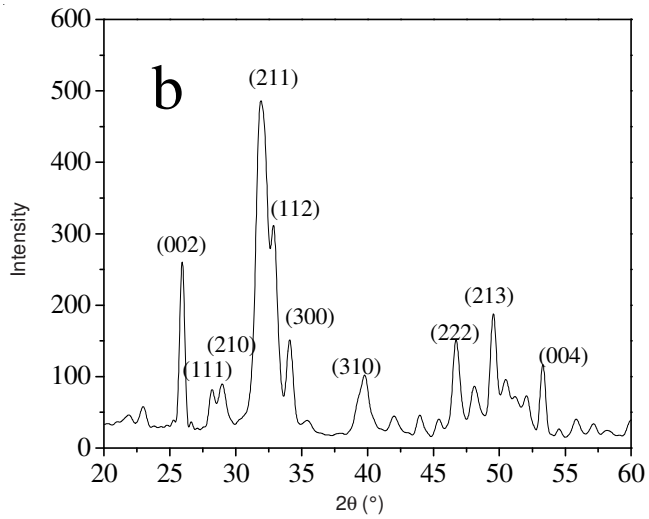

Fig. 1. TEM micrograph (a) and XRD pattern (b) of hydroxyapatite powders

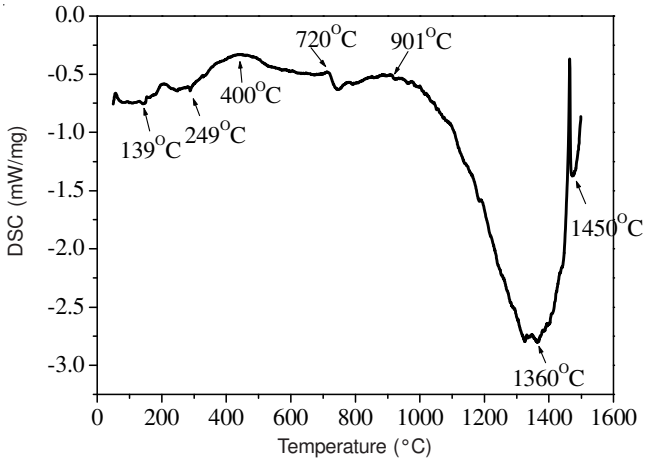

Fig. 2. High-temperature DSC curve of the nano-hydroxyapatite powders

hydroxyapatite. It is believed when the endothermic peak reached the maximum at 1360 ºC, hydroxyapatite dehydrates completely and is decomposing. The crystal phase transformation from β-TCP into α-TCP caused the last peak at 1450 ºC[15]. Higher decomposition temperature may delay the crystal phase transformation. The decomposition of hydroxyapatite powders can be described by the following equation.

$$Ca_{10}(PO_4)_6(OH)_2 \rightarrow 2Ca_3(PO_4)_2 + Ca_4P_2O_9 + H_2O \quad (1)$$

The decomposition behavior of the nano-hydroxyapatite powders was also studied by Raman spectroscopy at different temperatures. In Fig. 3, four Raman peaks located at 434, 594, 963 and 1047 cm^{-1} can be observed. The peak with the strongest intensity at 963 cm^{-1} is a characteristic peak of hydroxyapatite, corresponding to bond type ν_1(O-P-O). The other three peaks centered at 434, 594 and 1047 cm^{-1} are ascribed to ν_2(O-P-O), ν_4(O-P-O) and ν_3(P-O) bonds, respectively. The peak at 3569 cm^{-1} represents the characteristic vibrational peak for the hydroxyl group. The peak unfolds with temperature and the relative intensity decreases. Around 1000 ºC, the hydroxyl peak disappears completely. This result is consistent with that of DSC (Fig. 2), in which a large endothermic peak appears at 1000 ºC corresponding to its decomposition process. The peak representing PO_4^{3-} is still visible at 1350 ºC. Obviously, the decomposition process of hydroxyapatite starts with hydroxyl group, rather than the direct decomposition of the main structure. This fact means the binding capacity of PO_4^{3-} reduces and the system disorder increases. The highest temperature hydroxyapatite remained stable was detected as 1350 ºC by Raman spectroscopy. Table-1 summaries Raman peaks of hydroxyapatite. It can be seen that the key difference between hydroxyapatite and TCP is the presence of hydroxyl group in hydroxyapatite structure. In this work, results reveal that the nano-hydroxyapatite powders contain hydroxyl groups.

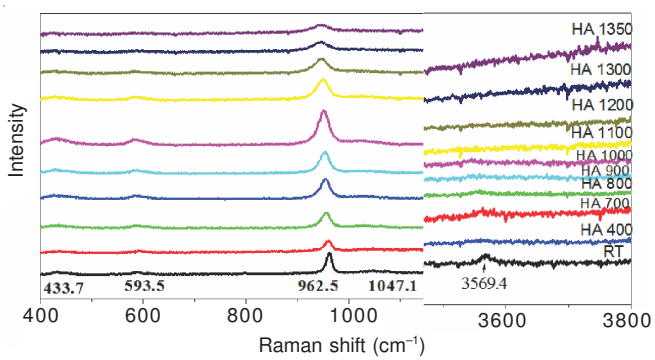

Fig. 3. High-temperature Raman spectra of the nano-hydroxyapatite powders

TABLE-1
RAMAN MODES OF HYDROXYLAPATITE (HA) AND α-TCP

	HA[13-16]	HA-COM[15,16]	α-TCP[16]
ν_2 (O-P-O)	432, 447	432, 445	420
ν_4 (O-P-O)	580, 593, 608	577, 590, 608	567
ν_1 (P-O-P)	948, 962	959	938
ν_3 (P-O)	1028,1053,1061,1075	1029,1046, 1072	1017
OH^-	3571	3571	–

It is observed that the relative intensity of the Raman peaks first increases and then decreases with the increase of temperature. Moreover, they shift to lower frequency field. As the temperature increases from 400-1000 ºC, the crystallinity of nano-hydroxyapatite powders increases and the corresponding peak intensity continuously enhances, which are consistent with the crystallization peaks shown in Fig. 2 by DSC. When the temperature is higher than 1000 ºC, the nano-hydroxyapatite powders decompose gradually. As a result, peaks broaden and peak intensity decreases, indicating that the long-range order of hydroxyapatite has been destroyed at that temperature through weakening the intermolecular binding force and loosing the molecular structures.

Raman spectra (Fig. 4) were measured at room temperature and by heating the nano-hydroxyapatite powders to 1500 ºC followed by cooling to room temperature. Compared to Fig. 3, the relative strength of ν_1(O-P-O) bond increases, while that of the ν_3(P-O) bond decreases. Their peak positions are essentially the same except for slight shift to the higher frequency field. Interestingly, the signal of hydroxyl groups stripped by heating appears again although the peak position slightly varies from 3569 to 3542 cm^{-1}. In addition, for hydroxyapatite cooled to room temperature the peak intensity of hydroxyl groups is lower than that of the original state of hydroxyapatite tested at room temperature. The above results indicate that high-temperature decomposition products of hydroxyapatite regenerate hydroxyl groups during the cooling process. Because the size effect of the nano-hydroxyapatite powder particles, they can fully contact and easily react with the moisture in the air when the furnace is cooling, illustrated by the following equation.

$$2Ca_3(PO_4)_2 + Ca_4P_2O_9 + H_2O \rightarrow Ca_{10}(PO_4)_6(OH)_2 \quad (2)$$

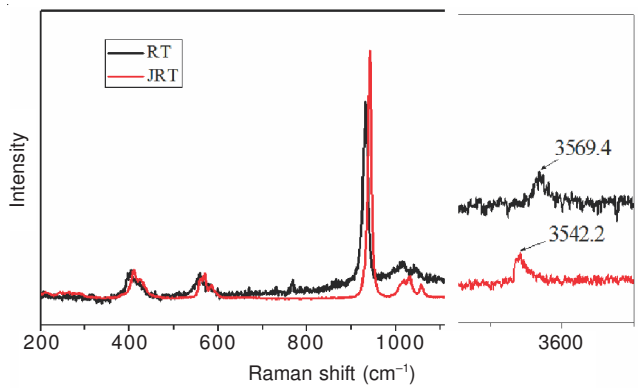

Fig. 4. Raman spectra of nano-hydroxyapatite powders at room temperature (RT: room temperature; JRT: cooling from 1500 ºC to room temperature)

It should be noted that Raman analysis of hydroxyapatite shows that hydroxyapatite decomposition is a reversible or partially reversible process. Therefore, how to take full advantage of the reversible process of hydroxyapatite to reproduce the biological activity of hydroxyapatite-products is clearly a meaningful issue.

Because hydroxyapatite is often applied in medical applications in the forms of block or coating, hydroxyapatite powders and the block after sintering at different temperatures were further analyzed by XRD. The results are shown in Figs. 5 and 6. In Fig. 5, in addition to the labeled β-TCP peak (β-TCP is the doping impurity in the preparation process), the rest peaks are arising from hydroxyapatite characteristic signals. Up to 1350 ºC, there is no obvious decomposition of the hydroxyapatite powders. This result is consistent with that from DSC and Raman analysis in this work as well as those reported in literatures[11,16]. From 400-800 ºC, the peaks obviously become clear and sharp, indicating the degree of crystallinity gradually becomes higher, which, in turn, supports the crystallization peaks in the DSC curves.

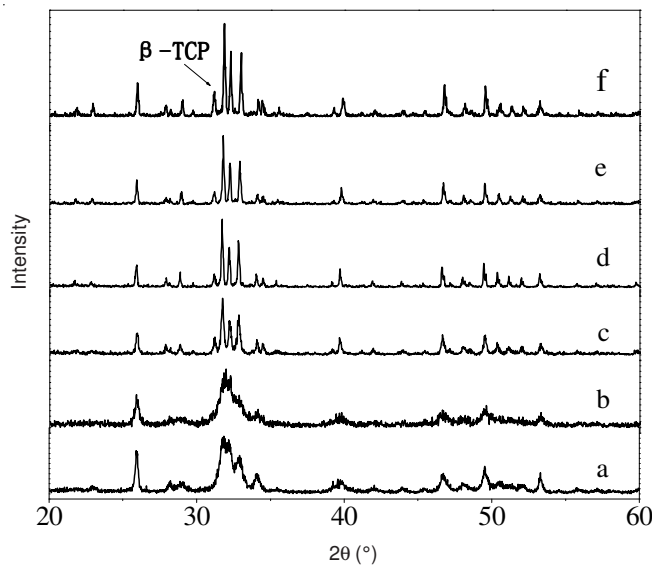

Fig. 5. XRD patterns of the nano-hydroxyapatite powders after sintering (a: original; b: 400 ºC; c: 800 ºC; d: 1000 ºC; e: 1200 ºC; f: 1350 ºC)

Fig. 6 shows the XRD patterns of hydroxyapatite powders and the sinters. The products of hydroxyapatite block after sintering at 1500 ºC are composed of α-TCP and TTCP. The peaks of the block and the powders sintered at 1300 ºC apparently are offset, which is due to the great pressure subjected by the pressed powder or another possibility that the decomposition temperature of the powder decreases. This phenomenon has not been reported previously and requires further investigation.

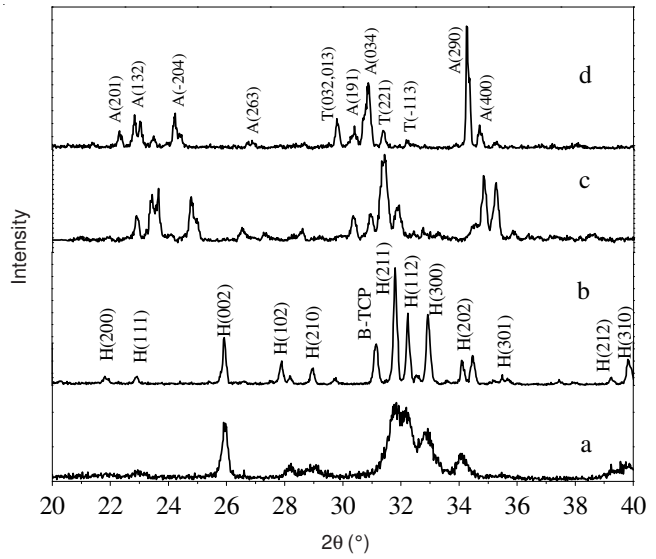

Fig. 6. Contrast of XRD patterns of hydroxyapatite powders and sinters (a: original powders; b: 1300 ºC powders; c: 1300 ºC sinters; d: 1500 ºC sinters)

We further explored the regeneration possibility of the hydroxyapatite block. The XRD results are shown in Fig. 7, which correspond to hydroxyapatite sinters at room temperature, regenerated at 900 ºC and decomposed. Compared with XRD patterns shown in Fig. 7(a-d) demonstrate that the hydroxyapatite was partially regenerated in the atmosphere

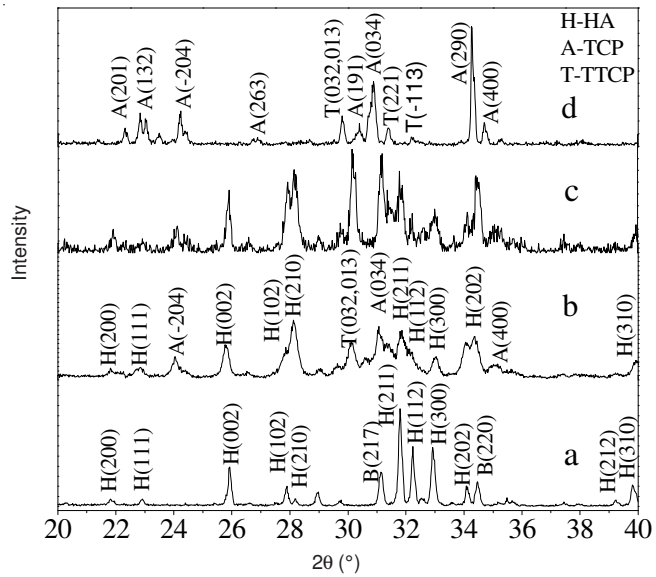

Fig. 7. XRD patterns of reconstructed hydroxyapatite (HA) sinters (a: RT; b: 900 ºC regeneration I; c: 900 ºC regeneration II; d: decomposed sinter)

conditions with addition of CaO and $Ca(OH)_2$. In Fig. 7(b-c), there are characteristic peaks like (002) (102) (210) (211) (112) (202), but a small amount of α-TCP still remains as confirmed by peaks at (-204) (034) (400). This may be related to the tight linkage between particles after being pressed and sintered into bulk which makes it impossible for the regeneration atmosphere to enter into the block. It is known that α-TCP can be converted to hydroxyapatite in the following two conditions[17-21].

$$3Ca_3(PO_4)_2 + CaO + H_2O \rightarrow Ca_{10}(PO_4)_6(OH)_2 \quad (3)$$

$$3Ca_3(PO_4)_2 + Ca(OH)_2 \rightarrow Ca_{10}(PO_4)_6(OH)_2 \quad (4)$$

Besides, compared to the curve shown in Fig. 7(b), the peak height in Fig. 7(c) is significantly higher, indicating the regeneration yield in sample c is larger than that in sample b. Regeneration increases with the increase in CO_2 and H_2O content in the atmosphere. Therefore, under suitable atmosphere the regeneration of hydroxyapatite block can occur partially. Combined with the results of regeneration of hydroxyapatite powders, it can be deduced that the regeneration of hydroxyapatite can be considered as a reversible reaction.

Conclusion

Hydroxyapatite gradually releases its OH^- from 1000 ºC and decomposes into β-TCP and TTCP when the heating temperature is higher than 1350 ºC. At 1450 ºC, β-TCP changes into α-TCP which remains if the sinter cools to the room temperature. When the hydroxyapatite sinter slowly cools to room temperature under a suitable atmosphere, the decomposed hydroxyapatite reconstitutes to hydroxyapatite. Heating at 900 ºC for 1 h, the sintered hydroxyapatite can be partially regenerated and the regeneration rate increases with H_2O content in the atmosphere.

ACKNOWLEDGEMENTS

The financial support from the Zhejiang Provincial Medical Research Foundation and Science and Technology Development Program of Hangzhou City are gratefully acknowledged.

REFERENCES

1. W. Suchanek and M. Yoshimura, *J. Mater. Res*., **13**, 94 (1998).
2. L.M. Sun, C.C. Berndt, K.A. Gross and A. Kucuk, *J. Biomed. Mater. Res*., **58**, 570 (2001).
3. S. Koutsopoulos, *J. Biomed. Mater. Res*., **62**, 600 (2002).
4. K. Mori, T. Hara, T. Mizugaki, K. Ebitani and K. Kaneda, *J. Am. Chem. Soc*., **126**, 10657 (2004).
5. L. Ji, G. Jell, Y. Dong, J.R. Jones and M.M. Stevens, *Chem. Commun*., **47**, 9048 (2011).
6. L.S. Wan, J.W. Li, B.B. Ke and Z.K. Xu, *J. Am. Chem. Soc*., **134**, 95 (2012).
7. A.J. Ruys, M. Wei, C.C. Sorrell, M.R. Dickson, A. Brandwood and B.K. Milthorpe, *Biomaterials*, **16**, 409 (1995).
8. A. Kalaivani, P. Satheeshkumar, G. Senguttuvan, V. Sivakumar and C. S. Dilip, *Asian J. Chem*., **25**, S324 (2013).
9. M.H. Fathi and E.M. Zahrani, *J. Alloys Comp*., **475**, 408 (2009).
10. G.M. Wu, W.D. Hsiao and S.F. Kung, *Surf. Coatings Technol*., **203**, 2755 (2009).
11. C.J. Liao, F.H. Lin, K.S. Chen and J.S. Sun, *Biomaterials*, **20**, 1807 (1999).
12. R. Quan, D. Yang, J. Yan, W. Li, X. Wu and H. Wang, *Mater. Sci. Eng. C*, **29**, 253 (2009).
13. F.-H. Lin, L. Chun-Jen, C. Ko-Shao and S. Jui-Sheng, *Mater. Sci. Eng. C*, **13**, 97 (2000).
14. M. Huang, J.Q. Feng, J.X. Wang, X.D. Zhang, Y.B. Li and Y.G. Yan, *J. Mater. Sci.-Mater. Med*., **14**, 655 (2003).
15. K. Kandori, S. Mizumoto, S. Toshima, M. Fukusumi and Y. Morisada, *J. Phys. Chem. B*, **113**, 11016 (2009).
16. L. Rintoul, E. Wentrup-Byrne, S. Suzuki and L. Grondahl, *J. Mater. Sci.-Mater. Med*., **18**, 1701 (2007).
17. A.F.L. Almeida, P.B.A. Fechine, J.M. Sasaki, A.P. Ayala, J.C. Goes, D.L. Pontes, W. Margulis and A.S.B. Sombra, *Solid State Sci*., **6**, 267 (2004).
18. C.C. Silva, A.G. Pinheiro, M.A.R. Miranda, J.C. Goes and A.S.B. Sombra, *Solid State Sci*., **5**, 553 (2003).
19. J.L. Xu and K.A. Khor, *J. Inorg. Biochem*., **101**, 187 (2007).
20. H. Li, B.S. Ng, K.A. Khor, P. Cheang and T.W. Clyne, *Acta Mater*., **52**, 445 (2004).
21. F.H. Lin, C.J. Liao, K.S. Chen and J.S. Sun, *Mater. Sci. Eng. C*, **13**, 97 (2000).